Improvement of the thermoelectric efficiency of pyrene-based molecular junction with doping engineering

Mohammad Farid Jamali[†], Meysam Bagheri Tagani[‡], and Hamid Rahimpour Soleimani[§]

Computational Nanophysics Laboratory (CNL), Department of Physics, University of Guilan, Rasht, P. O. Box 41335 – 1914, *Iran*

(Received 3 May 2017; revised manuscript received 13 June 2017; published online 20 November 2017)

In this study, the thermoelectric properties of pyrene molecule doped with boron and nitrogen atom at different sites of molecule are investigated using density functional theory and none-equilibrium Green's function formalism in the linear response regime. Our calculations show that when the impurities are added to the edge of the molecule, the anti-resonant peaks will appear in the transmission diagram in the vicinity of the Fermi energy level. So it increases the thermoelectric figure of merit of the system in comparison with the one that the impurity is located in the center of molecule. Additionally, the seebeck coefficient signs are not the same among the B, N, and N & B doped devices, indicating that the types of the carriers can be changed with different types of doping.

Keywords: thermopower, pyrene, density functional theory, none-equilibrium Green's function method, doping

PACS: 31.15.E–, 31.15.bt, 31.15.–p, 05.60.–k **DOI:** 10.1088/1674-1056/26/12/123101

1. Introduction

Last decades, the electronic devices have been fabricated with bulk materials such as silicon based technology. Since the miniaturization of this device approaches ti its physical limits, molecular junction, which is a branch of nanotechnology that uses single molecules or nanoscale collections of single molecules as electronic components, has been extensive studied, and during recent years it has gained great attention as an alternative to conventional semiconductor devices.[1–4]

The concept of molecular electronics was first published in 1974 when Aviram and Ratner suggested an organic molecule that could work as a rectifier.[5] The central issue in molecular electronic studies is to calculate the electron transport and thermoelectric properties through molecular junction.[6–10] About electronic transport properties, in recent two decades, current–voltage (I–V) characteristics of single molecular junction have been extensively studied with different types of molecules.[11–17] Such investigations provided a significant insight into charge transport through molecular junctions. In addition, it has been shown that the thermoelectricity provides useful information which cannot be obtained in the current–voltage measurements.[19,20] Thus, other important application of molecular junction, which is thermoelectricity, has been examined intensively because of some additional information that can be extracted from it such as types of carriers (p-type or n-type).[21,22] Thermoelectricity in the definition is the direct conversion between thermal and electric energy. By increasing thermopower coefficient and reducing thermal conductance, the thermoelectricity can be improved. Recent experiments show that molecular junction seems to lie in both aspects: (i) their thermopower coefficient should be large [23] due to resonant structure between the electron and the highest occupied molecular orbital (HOMO) or the lowest unoccupied molecular orbital (LUMO), and (ii) their thermal conductance is small[24] due to the mismatch between the electrodes and the molecule vibrational modes. So, a molecular junction is a good candidate for thermoelectric energy conversion and understanding the thermoelectric properties and therefore it is the central issue for molecular scale devices.

The thermoelectric efficiency of a system is described by the dimensionless figure of merit, $ZT = S^2 G_e T / \kappa$, where T is the average temperature of electrodes, S is the thermopower or seebeck coefficient, G_e is the electrical conductance, and κ is the thermal conductance which is for the total current including electronic and phononic heat current. But at low temperature (near room temperature) for organic molecular junctions, due to low overlap between the phonon modes of molecule and phonon modes of metallic electrodes the phonon thermal conductance can be ignored.[25,26] So, in this work we ignore the phononic thermal conductance and only consider the electron thermal conductance. In recent years, it was found that in nanostructures, such as thin-film and quantum dot superlattices, ZT can increase to about 1. Materials with $ZT \sim 1$ are regarded as having good thermoelectrics, but the materials with $ZT > 3$ would be required to compete with conventional refrigerators or generators.[27–29] Applications for ther-

[†]Corresponding author. E-mail: mfj_ss@yahoo.com
[‡]Corresponding author. E-mail: m_baghei33@yahoo.com
[§]Corresponding author. E-mail: rahimpour@guilan.ac.ir

© 2017 Chinese Physical Society and IOP Publishing Ltd

moelectrics cover a wide products areas such as the areas of medical, military, industrial, scientific/laboratory, and thermoelectric generators. For example, about thermoelectric generators, it has a variety of applications. Frequently, thermoelectric generators are used for low power remote applications or where bulkier but more efficient heat engines such as Stirling engines would not be possible.[30,31]

One of the important purposes of both theoretical and experimental researches on the molecular junction is to improve the magnitude of ZT. For this aim, some work has been done: (I) changing the connecting geometry or device configuration,[32–35] (II) considering different anchoring groups like amine, thiol, and carboxyl,[36–38] (III) attaching electron-donating or electron accepting side groups to the molecule,[39–42] and (IV) adding other atom to molecule as a doping case.[43–45] In this present work, we consider pyrene molecule ($C_{16}H_{10}$) as a single molecular device and examine the effect of adding boron and nitrogen atom as a doping in different sites on pyrene molecule in order to improve the magnitude of the ZT of pure pyrene. Pyrene is a parent class of polyclic aromatic hydrocarbons containing four fused ones. It is a well-known stable organic radical and is a kind of π-conjugated molecule that can be considered as a highly conductive molecular device. Pyrene can also be viewed as a small piece of graphene and used to fabricate the blocks for graphene nanosheets, too.[46] In recent years, many groups studied pyrene as electronic and also photonic devices and their electronic transport properties.[47–50] Xia *et al.* studied the effect of asymmetric contact geometry on the electronic transport properties of pyrene molecular device [51] and found that the asymmetric structures of both the molecule and the molecule–electrode couplings are responsible for the NDR behavior found in the I–V characteristics. Wu *et al.* designed a pyrene-ZGNR all-carbon device and investigate its spin-dependent transport properties.[52] Their results show that this system can exhibit multiple high performance spin-related properties, including spin filtering, spin rectifying, GMR and NDR effects, by modulating the magnetic field applied to electrodes. Fan *et al.* investigated the electronic transport properties of B- or N-doped pyrene molecule sandwiched between Au electrodes[53] and found that electronic transport properties are not constant and can be changed by shifting doped sites. Also, in recent years, studying the thermoelectric properties of molecular junctions like the thermopower and the thermoelectric figure of merit (ZT) has attracted much theoretical and experimental attention.[54–57] In the best of our knowledge, there is not any study on calculating thermoelectric properties of pyrene molecule especially in the presence of B and N doping. In this paper, thermoelectric features of pyrene molecule in connection to three-dimensional gold electrodes is investigated. Specially, we examine the effect of doping born and nitrogen atom on thermoelectric value. Seven models are considered, i.e., pyrene, x B dope, y B dope, x N dope, y N dope, x N & B doping, and y N & B doping corresponding to pure pyrene, pyrene dope with boron atom on the edge, pyrene dope with boron atom in the center, pyrene dope with nitrogen atom on the edge, pyrene dope with nitrogen atom in the center, pyrene dope with boron and nitrogen atom together on the edge and pyrene dope with boron and nitrogen atom in the center of pyrene molecule. The results show that adding all impurities at different sites will increase the thermoelectric figure of merit of pyrene molecule.

The rest of this paper is arranged in the following way. Section 2 is devoted to the system we investigate and the description of the NEGF–DFT method to calculate its thermoelectric properties. Section 3 presents our obtained numerical results for thermoelectric features of pyrene based molecule in the absence and the presence of B and N dope. Finally, we summarize the results in Section 4.

2. Computational methods

In this section, firstly we explain the detail of our junctions system and then present the formulation and methods to calculate the thermoelectric properties of molecular junctions. The pyrene is optimized by SIESTA code package[58] and after optimization, the optimized pyrene will connect to the gold electrodes. The model systems investigated in this work are demonstrated in Fig. 1. Device is divided into three regions: the left electrode, the central scattering region or central area, and the right electrode. The central scattering region includes a pyrene molecule which is bonded to two Au (111)-(4×4) electrode surfaces by using the thiol end group. The sulfur atom is chosen to be located at the hollow site of the gold triangle and the Au–S distance is 2.5 Å. In Fig. 1 we represent the geometry of our model consist of pure pyrene which can be replaced by other six modes; panel (a) for born dope at the edge (x) and center (y) site, panel (b) for nitrogen dope on edge (x) and y site, and panel (c) for nitrogen-born dope on edge (x) and y site. To calculate transmission coefficients we use the TRANSIESTA-C code.[59] The exchange correlation potential is described by the generalized-gradient approximation (GGA) proposed by Burke, Perdew and Ernzerhof. For organic atom the double-zeta plus polarization (DZP) basis set is considered and single-zeta plus polarization (SZP) basis set for the gold atoms are adopted and also plane-wave cut-off energy of 250 Ry (1 Ry = 13.6056923(12) eV) for the grid integration is chosen to present the accurate charge density. In the direct transfer, we consider the distance between the two

gold atoms to be 2.88 Å (gold lattice constant) and the other distance direction which is perpendicular to direct transfer to be 10 Å.[60]

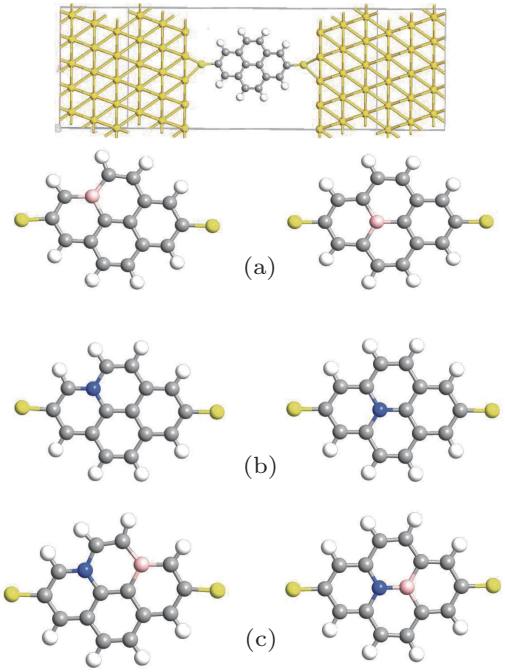


Fig. 1. (color online) Geometries of the molecular device in our simulation. Pyrene-based molecule with seven different forms is sandwiched between two gold electrodes. Pure pyrene, *x* B dope, *x* N dope, *y* B dope, *y* N dope, *x* N & B doping, and *y* N & B doping respectively.

In the following, to calculate the thermoelectric features of our system (metal-pyrene-metal junction), firstly the charge and heat currents are calculated by using the Keldish nonequilibrium Green function formalism which can be written as follows:[61,62]

$$I = \frac{e}{\hbar}\int \mathrm{d}\varepsilon T(\varepsilon)\left[f_{\mathrm{L}}(\varepsilon-\mu_{\mathrm{L}}) - f_{\mathrm{R}}(\varepsilon-\mu_{\mathrm{R}})\right],$$
$$I^{Q} = \frac{1}{\hbar}\int \mathrm{d}\varepsilon(\varepsilon-\mu)T(\varepsilon)\left[f_{\mathrm{L}}(\varepsilon-\mu_{\mathrm{L}}) - f_{\mathrm{R}}(\varepsilon-\mu_{\mathrm{R}})\right], \quad (1)$$

where $\hbar$ is the Planck constant,e is the electronic charge, $T(\varepsilon) = \mathrm{Tr}[\Gamma_{\mathrm{L}}(\varepsilon)G^{\mathrm{r}}(\varepsilon)\Gamma_{\mathrm{R}}(\varepsilon)G^{\mathrm{a}}(\varepsilon)]$ is the transmission coefficient of our system with Γ_{L} and Γ_{R} being the contact broadening functions associated with the left and right electrodes, G^{r} and G^{a} are the retarded and advance Green functions of the central region respectively, and f_{α} is the Fermi–Dirac distribution function of electrode α, μ_{L} and μ_{R} are the chemical potentials of left and right electrode respectively.

Since in this paper we study the thermoelectric properties in linear response regime, the charge current and thermal current are expanded by induced voltage, ΔV and temperature gradient, ΔT, to the first order[63]

$$I = \mathrm{e}^2 L_0 \Delta V + \frac{e}{T}L_1\Delta T,$$
$$I^{Q} = eL_1\Delta V + \frac{1}{T}L_2\Delta T, \quad (2)$$

where

$$L_n = -\frac{1}{\hbar}\int \mathrm{d}\varepsilon(\varepsilon-\mu)^n\frac{\partial f}{\partial\varepsilon}T(\varepsilon).$$

Also, from Eq. (2) the electric conductance G_{e} and the thermal conductance κ can be obtained as follows:

$$I = G_{\mathrm{e}}\Delta V \Rightarrow G_{\mathrm{e}} = \mathrm{e}^2 L_0,$$
$$I^{Q} = \kappa\Delta T \Rightarrow \kappa = \frac{1}{T}\left(L_2 - \frac{L_1^2}{L_0}\right). \quad (3)$$

Thermopower is the ratio of the induced voltage drop to the applied temperature gradient when the current is zero.

$$S = -\frac{\Delta V}{\Delta T} = -\frac{1}{eT}\frac{L_1}{L_0}. \quad (4)$$

As an aside, for energies close to Fermi energy, if $T(\varepsilon)$ varies only slowly with E on the scale of $\kappa_{\mathrm{B}}T$ then all of the above expression will take the well-known forms:[64,65]

$$G(T) \approx \left(\mathrm{e}^2\right)T(E_{\mathrm{F}}),$$
$$s \approx -\frac{\pi^2\kappa_{\mathrm{B}}^2 T}{3e}\frac{\partial\ln(T(E))}{\partial E}\Big|_E = E_{\mathrm{F}}, \quad (5)$$
$$\kappa \approx L_0 T G.$$

From the above equation for example, the thermopower is related to both the magnitude and the slope of the transmission function at the chemical potential of the contact (E_{F} for metal contact).

3. Results

Figure 2 shows the plots of logarithm of transmission coefficient versus energy for our seven models. Several conclusions can be extracted from this figure: i) For pure pyrene (pyrene without any doping), the HOMO (highest occupied molecular orbital) peak is broader than that of LUMO (lowest unoccupied molecular orbital) and the HOMO–LUMO gap (HLG) is more than 2.5 eV which is less than the gap reported in Ref. [53]. Here, we consider GGA approximation for exchange–correlation potential that underestimates HLG, whereas the LDA approximation was used in Ref. [53]. The transmission in Fermi energy is very little and its peak is far from it and just the tail of transmission peak extends to the Fermi energy level. ii) When born atom dopes to pyrene molecule on the x site, that is, in negative energy and very close to Fermi energy we can see a resonant peak which is related to interference effect and backscattering due to born atom. From the figure, in this case we can see a broad transmission coefficient in an energy range from -0.3 eV to -1.5 eV. iii) At the x site when we replace the born atom with nitrogen atom, the transmission peaks are replaced so that the dominant peak can be seen in the positive energy (between 0.3 to 1.5) or the resonant peak is visible near the Fermi energy and in positive energy. Apparently, B doping moves the

HOMO level close to the Fermi energy and LUMO level far from it while N doping moves the LUMO close to Fermi energy and HOMO level far from it. In addition, the resonant peak for B doping which is in negative energy is bigger than that for N doping which is in positive energy that can be attributed to electron donating and electron withdrawing nature of N and B. iv) By changing the doping position from x to y, the interaction effect will be increased and we can see an anti-resonance peak ($\tau = 0$) in $E = \pm 0.8$ eV which is in negative energy for B and in positive energy for N doping. v) By adding two impurities (B and N) simultaneously, the HOMO and LUMO levels move with respect to the Fermi energy. In this case, increasing the interaction which is due to the increasing of impurities will reduce the transmission coefficient peak in comparison with one impurity (B or N) mode. However, it is more than the non-doping case yet. About position of doping, for x position where N and B are closer to the left and right electrodes than for the y position, the transmission value is smaller because it provides more dispersion for incident electron wave. In addition, the slope of the logarithm of the transmission close to the Fermi energy will increase which leads to thermopower value bigger than that in the non-doping case.

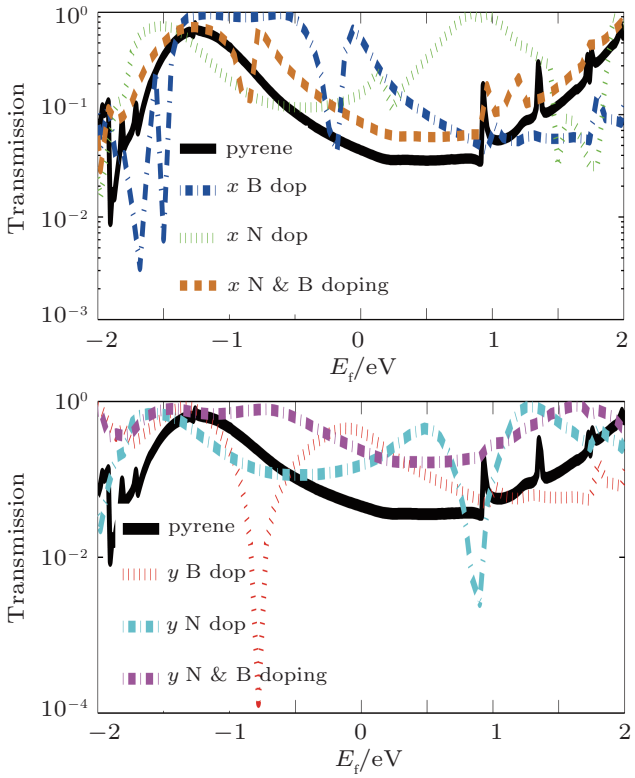


Fig. 2. (color online) Plots of transmission coefficient versus energy for seven models.

Figure 3 shows the plots of the thermopower versus temperature for our seven models. Results are as follows: a) For temperature above 100 K, adding impurity to molecule will increase the thermopower so that the maximum change is related to doping at the x site. b) When a boron atom dopes to pyrene molecule, the thermopower sign becomes positive which indicates p-type conduction and charge carriers are holes. Also, in this case the Fermi level is close to HOMO level and located in small HOMO-LUMO gap. And if the boron atom is located at the x site, the thermopower amount increases and we can see the maximum value for S. c) Adding nitrogen on both x and y sites will cause the thermopower to become negative which expresses the fact that the Fermi level is located in big HOMO–LOMO gap (in comparison to B dope) and is close to LUMO level (see Fig. 2). In this case electrons are charge carriers and indicating n-type conduction. The results are consistent with electron-donating and electron-withdrawing nature of nitrogen and born, respectively. d) When we dope boron and nitrogen simultaneously to pyrene molecule, the thermopower sign becomes positive again. In this case, the thermopower value for N & B doping at the y site is bigger than at the x site, however, when boron or nitrogen separately dopes to the molecule, the thermopower value for x site becomes bigger than for the y site. It should be noted that our obtained maximum magnitude of thermopower for x B dope is more than that of reported in Refs. [66] and [67].

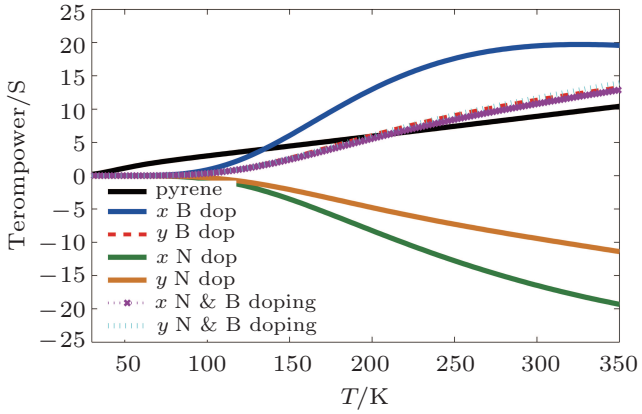


Fig. 3. (color online) Plots of thermopower versus temperature.

In addition, to elucidate the cause of change in thermopower sign and value due to adding N and B to pyrene molecule, from Eq. (5) we have to see Fig. 2. Because near the Fermi level, the thermopower is proportional to the slope of the logarithm of transmission coefficient. According to Fig. 2 when the nitrogen dopes, the slope of transmission plot $[\partial \ln(\tau(\varepsilon))/\partial\varepsilon]$ is positive so from the equation the thermopower become negative. Also in this case, the slope of x N dope is bigger than that of y N dope and for this reason the magnitude of thermopower for x N dope is bigger. For other cases the slopes of the transmission curve are negative which will cause the thermopower sign to become positive. Also, the slope for x B dope is maximum so we can see the maximum thermopower for it. Besides, if we plot the curves of

transmission very close to the Fermi level we can see an anti-resonant peak for x B dope and x N dope (see Fig. 4) since the anti-resonant peak or transmission node increases the logarithmic derivative,[68] the thermopower magnitude can be enhanced by using anti-resonant peak, and the maximum magnitude for thermopower is related to the adding of B and N dope to pyrene at the x site respectively.

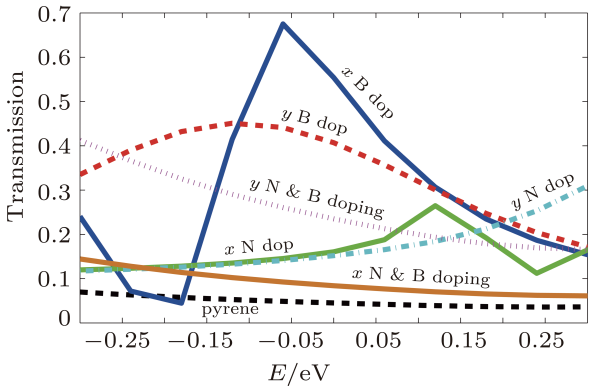


Fig. 4. (color online) Plots of transmission coefficient very close to Fermi energy.

To elucidate the electrodes chemical potential displacement on the Seebeck coefficient, in Fig. 5 we calculate the thermopower as a function of chemical potential at $T = 300$ K. As one can see, adding impurities to pyrene molecule will create a prominent resonance peak in the diagram of thermopower. So if the impurity is added to the x site (at the edges and away from the center) the peak appears near the zero chemical potential (Fermi level) while it is located at the y site (at the center) the corresponding peak will be created away from the Fermi level. For born doping the peak is located in negative chemical potential while for nitrogen the peak site will transfer to positive chemical potential that can be related to the electron donating and electron accepting nature of nitrogen and born respectively. In fact, the chemical potential sign indicates the doping level of the system.[69] For n-doping (nitrogen atom) the Fermi level shifts up and for p-type doping (born atom) the Fermi level is lowered in comparison with the zero chemical potential. In addition, we can see the oscillatory behavior for S and since the height of the peak at the y site is bigger than at the x site for both N and B dopes, the oscillatory behavior in the y site is more than that of x one. However, when the born atom and nitrogen simultaneously dope to the pyrene molecule, the oscillatory behavior only appear at the x N & B doping case and in negative energy and far from the Fermi level. Also, in this case the height of peak is small in comparison with the case of N or B dope alone. Beside, when the thermopower is zero it has two means. 1) At these points the slopes of transmission are all zero. For example, about y N & B doping as can be seen from Fig. 4 the slope of transmission is very little in the vicinity of Fermi energy and become zero in the energy range between -0.6 eV to -1.3 eV. So we can also see this behavior in the thermopower diagram, and for this reason the thermopower value for y N & B doping is very little and almost zero. 2) At these points the Fermi level crosses the HOMO–LUMO orbital and the molecular orbital changes from electron-dominated to hole-dominated transport thus the thermopower sign changes. Also, at these points the following relation is established:

$$\left.\frac{\partial \ln \tau(\varepsilon)}{\partial \varepsilon}\right|_{\varepsilon=\mu_{\mathrm{L}}} = -\left.\frac{\partial \ln \tau(\varepsilon)}{\partial \varepsilon}\right|_{\varepsilon=\mu_{\mathrm{R}}}.$$

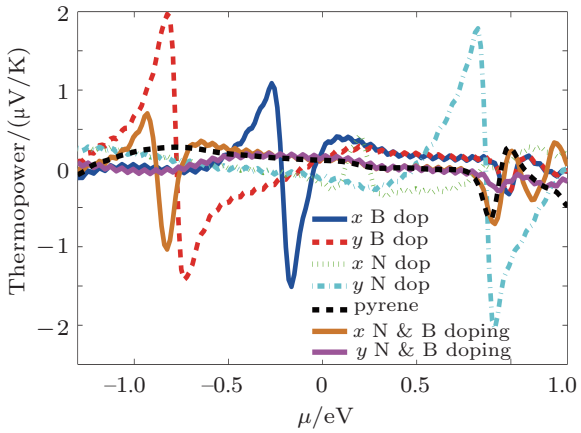


Fig. 5. (color online) Plots of thermopower versus chemical potential for our seven models.

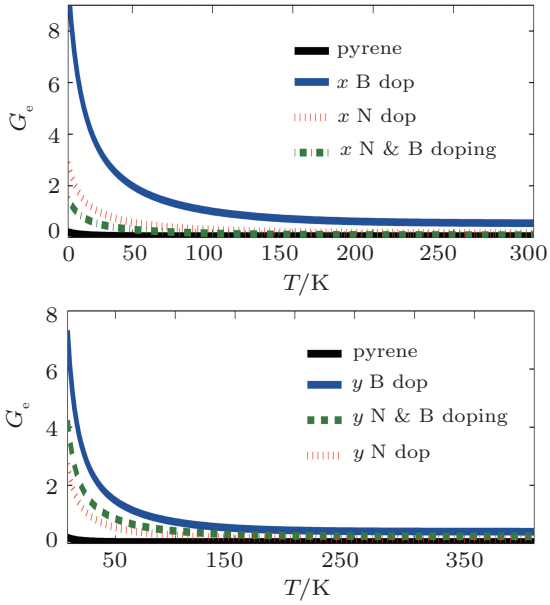


Fig. 6. (color online) Plots of the electrical conductance versus temperatures.

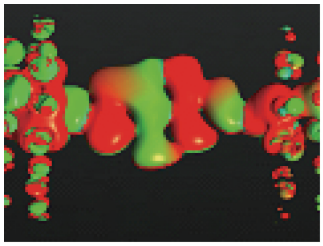
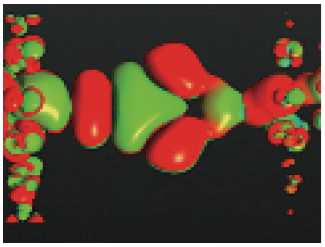
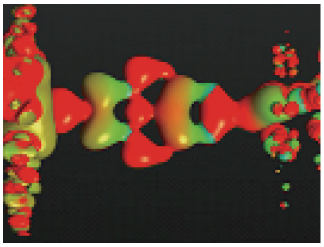
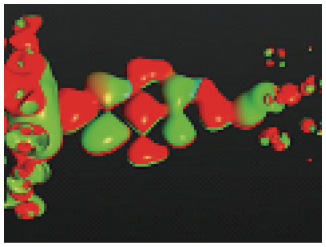
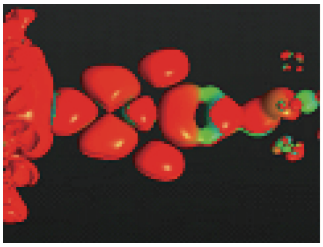
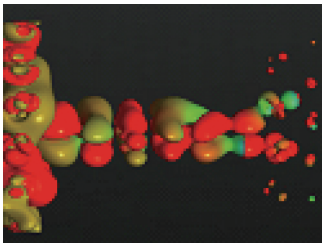
Figure 6 shows the plots of electrical conductance (G_{e}) against temperature for pyrene molecular junction with and without doping. Several conclusions in the evaluation of G_{e} can be obtained. 1) Adding N and B doping to the pyrene molecule (at the x and y sites) will increase the magnitude of the electrical conductance of which the maximum is for B doping at the x site and minimum is for N & B doping at the x site; 2) When boron and nitrogen impurities individually are at x

site, the electrical conductivity is bigger than at the y site. But when we dope simultaneously N and B at the x and y sites, the value of G_e at the y site becomes bigger than at the x site. To clarify this issue, we calculate the transmission eigenvalues and eigenstates for the different doping configurations at zero energy, as indicated in Tables 1 and 2, respectively. Results show that the best crossing channel for electron transport is in the x-B doping case and the worst one is for the x N & B doping case. This conclusion is evident as shown in Fig. 4. Transmission eigenstate spectrum is completely delocalized for the x-B case resulting in the high electrical conductance. In contrast, the spectrum of the x-N & B doping one is localized, leading to the low electrical conductance. Phase transition from delocalization to localization in the transmission spectrum is equivalent to the significant reduction in the electrical conductance. 3) At temperatures below the 150 K, by increasing the temperature the value of the G_e exponentially decreases for all structures because at the positions close to the Fermi energy the transmission coefficient does not change significantly but when the temperature increases, the Fermi derivative peak height is reduced. After temperature 150 K, the electrical conductance reaches its saturation value and becomes temperature-independent.

Table 1. Eigenvalues calculated at zero energy for different doping modes.

Doping type	x N & B doping	y N dope	x N dope	y N & B doping	Y B dope	x B dope
Eigenvalue	0.1	0.18	0.19	0.3	0.43	0.61

Table 2. Eigen-states calculated at zero energy for different doping modes.

x B dope	y B dope	y N & B doping
		
		
x N dope	y N dope	x N & B doping

In the following, we examine the variations of the electron thermal conductivity behavior with temperature and chemical potential. It should be noted that according to Eq. (3), thermal conductivity depends on two terms, i.e., L_2 and L_1^2/L_0. But our calculations show that for all 7 structures studied in the article, according to the values of these two terms, we can ignore L_1^2/L_0 in comparison with L_2. So, the term L_2 is fundamental in our calculations that can be calculated from

$$L_2 = -\frac{1}{h}\int \mathrm{d}\varepsilon(\varepsilon-\mu)^2\frac{\partial f}{\partial \varepsilon}\tau(\varepsilon).$$

Firstly, in Fig. 7(a) the plots of the thermal conductivity against temperature are shown for seven junctions. Only the term that changes with temperature in the above equation is the Fermi derivative which is broaden with the increase of temperature and thus covers more parts of the transmission coefficient near the Fermi level and therefore, the number of carriers participating in transport will increase. According to the transmission diagram in Fig. 2, the peak height near the Fermi level for the x B dope is higher than for other models. So, the increase of thermal conductivity is more sensible to temperature. Figures. 7(b) and 7(c) show the Fermi derivatives for the x B dope and the x N & B doping, which have the maximum and minimum change with temperature.

As can be seen from the figure, the existence of a resonant peak at the Fermi level for x B-dope significantly increases the electronic thermal conductance. In contrast, the peak of

transmission coefficient is far from the Fermi level for x-N & B doping case, so, the thermal conductance is low. It is interesting to note that the pure pyrene junction has the lowest electronic thermal conductivity.

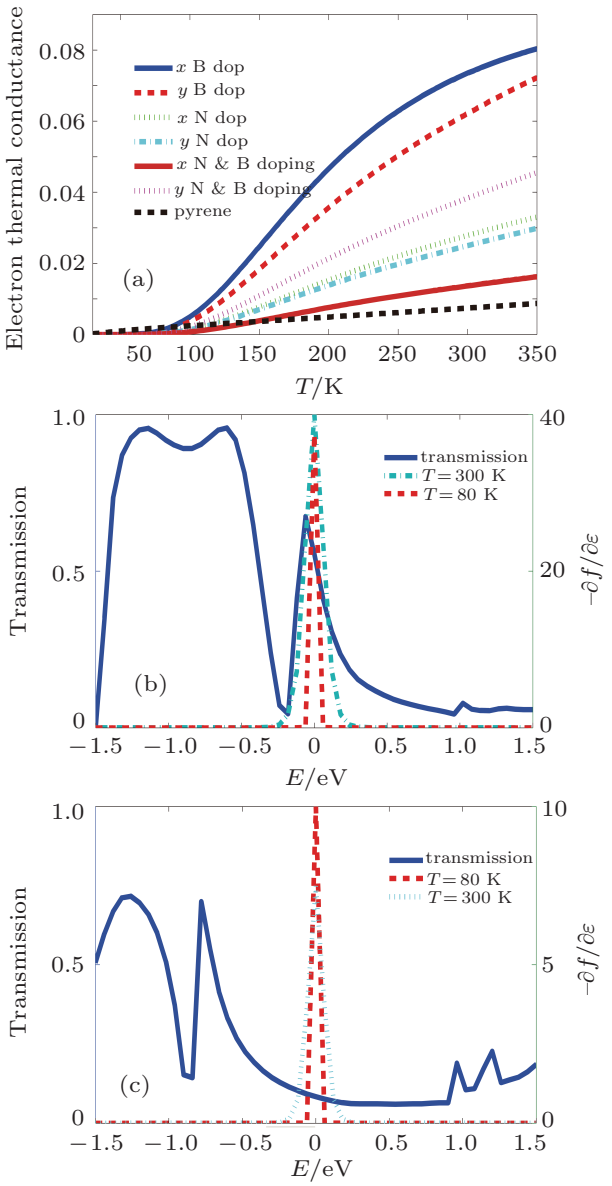


Fig. 7. (color online) (a) Plots of electron thermal conductance versus temperatures. (b) Fermi derivative change with temperature for x B dope. (c) Fermi derivative change with temperature for x N & B doping dope.

Figure 8(a) shows the thermal conductance against chemical potential. The different behaviors of thermal conductance in terms of chemical potential are due to the variation of the transmission coefficient with energy. For example for x B dope as can be seen from Fig. 8(b) for energies of -0.05 eV and -0.8 eV, the transmission coefficient peak is located in the $-\partial f/\partial\varepsilon$ window and the product of $(\varepsilon-\mu)^2(-\partial f/\partial\varepsilon)\tau(\varepsilon)$ increases. Therefore, the L_2 and the thermal conductance magnitude increase in these energies. Besides, for negative energies away from the chemical potential, due to the larger values of $(\varepsilon-\mu)^2$ the thermal conductance becomes larger. While with a positive energy of 1 eV for example, the insignificant magnitude of transmission coefficient is located in the $-\partial f/\partial\varepsilon$ window and for this reason the thermal conductance is lower in these range of energy.

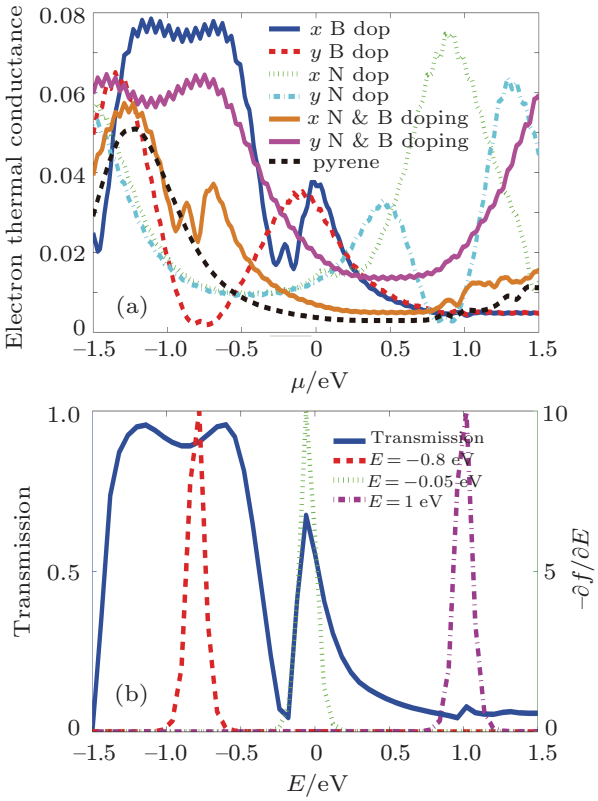


Fig. 8. (color online) (a) Plots of electron thermal conductance versus chemical potential. (b) Different chemical potential windows for x B dope.

Finally, we calculate the figure of merit (ZT) as a function of temperature (as shown in Fig. 9). As it is visible adding impurities to pyrene molecule at both places x and y will increase the magnitude of the ZT in comparison with pure pyrene molecular junction. Due to the dependence of the ZT on the electrical and thermal conductance and the thermopower, its behavior varies nonlinearly with the increase of temperature. The maximum of ZT for x B dope case is around 0.01, which is obtained at room temperature (300 K). Beside, for all junctions the ZT will increase with the increase of temperature.

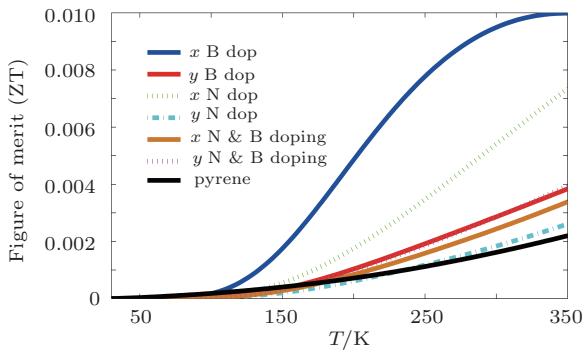


Fig. 9. (color online) Plots of thermoelectric figure of merit (ZT) versus temperature.

The experimental magnitude of the ZT for the pyrene molecule has not been reported in the literature before, but in comparison with other work on molecular junctions, the ZT obtained in this work for the case of x-B dope is comparable to the one reported in Ref. [70] for paracyclophane-based single-molecule junctions.

4. Conclusions

In this article, by combining the nonequilibrium Green function method with density functional theory, we studied the thermoelectric features of the pyrene-based molecular junction. We also analyzed theoretically the effect of adding boron atom and nitrogen atom as impurities in different sites of the molecule, on the thermoelectric properties of pyrene molecule. Our calculation shows that when B and N atoms dope to the molecule at the different sites, the thermoelectric properties will increase and we can see better thermopower and figure of merit of pure pyrene. The maximum increase is for x B dope case which is due to appearing anti-resonant peak very close to Fermi energy in transmission coefficient which does not appear in the case of the pure pyrene. In addition, the thermopower signs for N dope at both places are negative, which indicates n-type conduction and shows that charge carriers are electrons while for other case the thermopower sign becomes positive which indicate p-type transport and shows that the charge carriers are hole.

References

[1] Taylor J, Guo H and Wang J 2001 *Phys. Rev. B* **63** 245407
[2] Dubi Y and Di Ventra M 2008 *Nano Lett.* **9** 97
[3] Zhou J, Chen F and Xu B 2009 *J. Am. Chem. Soc.* **131** 10439
[4] Xu B 2007 *Small* **3** 2061
[5] Aviram A and Ratner M A 1974 *Chem. Phys. Lett.* **29** 277
[6] Tsutsui M and Taniguchi M 2012 *Sensors* **12** 7259
[7] Zimbovskaya N A and Pederson M R 2011 *Phys. Rep.* **509** 1
[8] Leijnse M, Wegewijs M R and Flensberg K 2010 *Phys. Rev. B* **82** 045412
[9] Tan A, Balachandran J, Sadat S, Gavini V, Dunietz B D, Jang S Y and Reddy P 2011 *J. Am. Chem. Soc.* **133** 8838
[10] Tao N J 2006 *Nat. Nanotechnol.* **1** 173
[11] Wang C K and Luo Y 2003 *J. Chem. Phys.* **119** 4923
[12] Tan A, Sadat S and Reddy P 2010 *Appl. Phys. Lett.* **96** 013110
[13] Reddy P, Jang SY, Segalman R A and Majumdar A 2007 *Science* **315** 1568
[14] Thygesen K S 2008 *Phys. Rev. Lett.* **100** 166804
[15] Zhang Z, Yang Z, Yuan J, Zhang H, Ming Q and Deng X 2009 *Solid State Commun.* **149** 60
[16] Tan A, Sadat S and Reddy P 2010 *Appl. Phys. Lett.* **96** 013110
[17] Darancet P, Widawsky J R, Choi H J, Venkataraman L and Neaton J B 2012 *Nano Lett.* **12** 6250
[18] Wagner S, Kisslinger F, Ballmann S, Schramm F, Chandrasekar R, Bodenstein T, Fuhr O, Secker D, Fink K, Ruben M and Weber H B 2013 *Nat. Nanotechnol.* **8** 575
[19] Zahid F, Ghosh A W, Paulsson M, Polizzi E and Datta S 2004 *Phys. Rev. B* **70** 245317
[20] Reddy P, Jang S Y, Segalman R A and Majumdar A 2007 *Science* **315** 1568
[21] Paulsson M and Datta S 2003 *Phys. Rev. B* **67** 241403
[22] Leijnse M, Wegewijs M R and Flensberg K 2010 *Phys. Rev. B* **82** 045412
[23] Pauly F, Viljas J K, Brkle M, Dreher M, Nielaba P and Cuevas J C 2011 *Phys. Rev. B* **84** 195420
[24] Dubi Y 2013 *New J. Phys.* **15** 105004
[25] Bergfield J P, Solis M A and Stafford C A 2010 *ACS Nano* **4** 5314
[26] Golsanamlou Z, Tagani M B and Soleimani H R 2015 *Phys. Chem. Chem. Phys.* **17** 13466
[27] Vining C B 2009 *Nat. Mater.* **8** 83
[28] Ke S H, Yang W, Curtarolo S and Baranger H U 2009 *Nano Lett.* **9** 1011
[29] Harman T C, Taylor P J, Walsh M P and LaForge B E 2002 *Science* **297** 2229
[30] Baranowski, L L, Warren E L and Toberer E S 2014 *J. Electron. Mater.* **43** 2348
[31] Kraemer D, Poudel B, Feng H P, Caylor J C, Yu B, Yan X, Ma Y, Wang X, Wang D, Muto A and McEnaney K 2011 *Nat. Mater.* **10** 532
[32] Fan Z Q and Chen K Q 2010 *Appl. Phys. Lett.* **96** 053509
[33] Zang Y, Li C Z, Chueh C C, Williams S T, Jiang W, Wang Z H, Yu J S and Jen A K Y 2014 *Adv. Mater.* **26** 5708
[34] Xue Y and Ratner M A 2004 *Phys. Rev. B* **69** 085403
[35] Chen F, Li X, Hihath J, Huang Z and Tao N 2006 *J. Am. Chem. Soc.* **128** 15874
[36] Baheti K, Malen J A, Doak P, Reddy P, Jang S Y, Tilley T D, Majumdar A and Segalman R A 2008 *Nano Lett.* **8** 715
[37] Kiguchi M, Nakamura H, Takahashi Y, Takahashi T and Ohto T 2010 *J. Phys. Chem. C* **114** 22254
[38] Balachandran J, Reddy P, Dunietz B D and Gavini V 2012 *J. Phys. Chem. Lett.* **3** 1962
[39] Taylor J, Brandbyge M and Stokbro K 2003 *Phys. Rev. B* **68** 121101
[40] Ernzerhof M, Zhuang M and Rocheleau P 2005 *J. Chem. Phys.* **123** 134704
[41] Finch C M, Garcia-Suarez V M and Lambert C J 2009 *Phys. Rev. B* **79** 033405
[42] Stadler R and Markussen T 2011 *J. Chem. Phys.* **135** 154109
[43] Nozaki D, Sevinli H, Li W, Gutirrez R and Cuniberti G 2010 *Phys. Rev. B* **81** 235406
[44] Kim G H, Shao L, Zhang K and Pipe K P 2013 *Nat. Mater.* **12** 719
[45] Ho P K, Kim J S, Burroughes J H, Becker H, Li S F, Brown T M Cacialli F and Friend R H 2000 *Nature* **404** 481
[46] Chen D M, Shenai P M and Zhao Y 2011 *Phys. Chem. Chem. Phys.* **13** 1515
[47] Bauschlicher C W, Ricca A, Xue Y and Ratner M A 2004 *Chem. Phys. Lett.* **390** 246
[48] Rastkar A, Ghavami B, Jahanbin J, Afshari S and Yaghoobi M 2015 *J. Comput. Electron.* **14** 619
[49] Zhang H, Zeng J and Chen K Q 2012 *Physica E: Low-dimensional Systems and Nanostructures* **44** 1631
[50] Wang Y, Wang H, Liu Y, Di C A, Sun Y, Wu W, Yu G, Zhang D and Zhu D 2006 *J. Am. Chem. Soc.* **128** 13058
[51] Xia C J, Liu D S, Liu H C and Zhai X J 2011 *Physica E: Low-dimensional Systems and Nanostructures* **43** 1518
[52] Wu Q, Zhao P and Liu D 2016 *RSC Adv.* **6** 16634
[53] Fan Z Q, Zhang Z H, Qiu M, Deng X Q and Tang G P 2012 *Appl. Phys. Lett.* **101** 073104
[54] Widawsky J R, Darancet P, Neaton J B and Venkataraman L 2011 *Nano Lett.* **12** 354
[55] Reddy P, Jang S Y, Segalman R A and Majumdar A 2007 *Science* **315** 1568
[56] Schneebeli S T, Kamenetska M, Cheng Z, Skouta R, Friesner R A, Venkataraman L and Breslow R 2011 *J. Am. Chem. Soc.* **133** 2136
[57] Pai W W, Jeng H T, Cheng C M, Lin C H, Xiao X, Zhao A, Zhag X, Xu G, Shi X Q, Van Hove M A and Hsue C S 2010 *Phys. Rev. Lett.* **104** 036103
[58] Soler J M, Artacho E, Gale J D, Garca A, Junquera, J, Ordejn P and Snchez-Portal D 2002 *J. Phys.: Condens. Matter* **14** 2745
[59] Pack J D and Monkhorst H J 1977 *Phys. Rev. B* **16** 1748

[60] An Y P, Yang C L, Wang M S, Ma X G and Wang D H 2009 *J. Chem. Phys.* **131** 024311

[61] Zahid F, Paulsson M, Polizzi E, Ghosh A W, Siddiqui L and Datta S 2005 *J. Chem. Phys.* **123** 064707

[62] Haug H and Jauho A P 2008 *Quantum Kinetics in Transport and Optics of Semiconductors*, pp. 181–212

[63] Golsanamlou Z, Vishkayi S I, Tagani M B and Soleimani H R 2014 *Chem. Phys. Lett.* **594** 51

[64] Wang B, Xing Y, Wan L, Wei Y and Wang J 2005 *Phys. Rev. B* **71** 233406

[65] Paulsson M and Datta S 2003 *Phys. Rev. B* **67** 241403

[66] Liu Y S, Chen Y R and Chen Y C 2009 *ACS Nano* **3** 3497

[67] Wang Z, Xie R, Bui C T, Liu D, Ni X, Li B and Thong J T 2010 *Nano Lett.* **11** 113

[68] Garca-Surez V M, Lambert C J, Manrique D Z and Wandlowski T 2014 *Nanotechnology* **25** 205402

[69] Lv H Y, Liu H J, Pan L, Wen Y W, Tan X J, Shi J and Tang X F 2010 *J. Phys. Chem. C* **114** 21234

[70] Brkle M, Hellmuth T J, Pauly F and Asai Y 2015 *Phys. Rev. B* **91** 165419